Mass spectrometer calibration of Cosmic Dust Analyzer

Thomas J. Ahrens, Satish C. Gupta,[1] and G. Jyoti[1]

Lindhurst Laboratory of Experimental Geophysics, Seismological Laboratory, California Institute of Technology, Pasadena, California, USA

J. L. Beauchamp

Arthur Amos Noyes Laboratory of Chemical Physics, California Institute of Technology, Pasadena, California, USA

Received 11 April 2002; revised 24 July 2002; accepted 28 August 2002; published 14 February 2003.

[1] The time-of-flight (TOF) mass spectrometer (MS) of the Cosmic Dust Analyzer (CDA) instrument aboard the Cassini spacecraft is expected to be placed in orbit about Saturn to sample submicrometer-diameter ring particles and impact ejecta from Saturn's satellites. The CDA measures a mass spectrum of each particle that impacts the chemical analyzer sector of the instrument. Particles impact a Rh target plate at velocities of 1-100 km/s and produce some 10^{-8} to 10^{-5} times the particle mass of positive valence, single-charged ions. These are analyzed via a TOF MS. Initial tests employed a pulsed N_2 laser acting on samples of kamacite, pyrrhotite, serpentine, olivine, and Murchison meteorite induced bursts of ions which were detected with a microchannel plate and a charge sensitive amplifier (CSA). Pulses from the N_2 laser (10^{11} W/cm^2) are assumed to simulate particle impact. Using aluminum alloy as a test sample, each pulse produces a charge of $\sim$4.6 pC (mostly Al^{+1}), whereas irradiation of a stainless steel target produces a $\sim$2.8 pC (Fe^{+1}) charge. Thus the present system yields $\sim 10^{-5}$% of the laser energy in resulting ions. A CSA signal indicates that at the position of the microchannel plate, the ion detector geometry is such that some 5% of the laser-induced ions are collected in the CDA geometry. Employing a multichannel plate detector in this MS yields for Al-Mg-Cu alloy and kamacite targets well-defined peaks at 24 (Mg^{+1}), 27(Al^{+1}), and 64 (Cu^{+1}) and 56 (Fe^{+1}), 58 (Ni^{+1}), and 60 (Ni^{+1}) dalton, respectively. *INDEX TERMS:* 2129 Interplanetary Physics: Interplanetary dust; 3944 Mineral Physics: Shock wave experiments; 5420 Planetology: Solid Surface Planets: Impact phenomena (includes cratering); 5465 Planetology: Solid Surface Planets: Rings and dust; 6015 Planetology: Comets and Small Bodies: Dust; *KEYWORDS:* Cosmic Dust Analyzer, Cassini, mass spectrometer, laser ionization, impact ionization

Citation: Jyoti, G., S. C. Gupta, T. J. Ahrens, and J. L. Beauchamp, Mass spectrometer calibration of Cosmic Dust Analyzer, *J. Geophys. Res.*, *108*(E2), 5007, doi:10.1029/2002JE001912, 2003.

1. Introduction

[2] The Cassini mission, an international cooperation venture, was launched in October 1997. One of the objectives of this mission is to characterize the dust particles at the planet Saturn, within and between the rings, and surrounding its icy satellites. It arrives at Saturn in 2004. For this purpose the Cassini spacecraft is equipped with a Cosmic Dust Analyzer (CDA). The region of space to be studied and the details of the ion detection systems on CDA are described by *Grün et al.* [1985]. The CDA is expected to make in situ measurements of the charge (10^{-15} – 10^{-12} C), the impact speeds, the mass and composition of these dust particles. The micrometeoroid mass measurement range is 10^{-16} to 10^{-6} g and the speed measurement range is 1 to 100 km/s. The charge on the particles is measured upon their passage through the two inclined grids at the entrance of the sensor housing, Figure 1a. An integrated time-of-flight impact ionization mass spectrometer (Chemical Analyzer) provides constraints on the particle chemical composition [*Spilker*, 1997]. Particles impacting onto the Rh target plate of this instrument and some mass of the target itself get vaporized and partially ionized. The positive ions, mostly singly charged so produced, are accelerated to 10^3 eV and are then collected upon traveling some 25 cm in a drift tube within the CDA. Providing no equi-dalton interference exists, the time of arrival of ions provide mass spectra for each dust particle in the above mass range.

[3] The CDA has two types of ion detection systems [*Srama and Grün*, 1997]; one is an electron multiplier and the other is a charge sensitive amplifier (CSA) that measures the total charge (positive) that is neutralized by electrons corresponding to the ions collected at the ion collector. The electron multiplier (Johnston, type MM1) consists of

[1]Now at High Pressure Physics Division, Bhabha Atomic Research Center, Mumbai, India.

Copyright 2003 by the American Geophysical Union.
0148-0227/03/2002JE001912

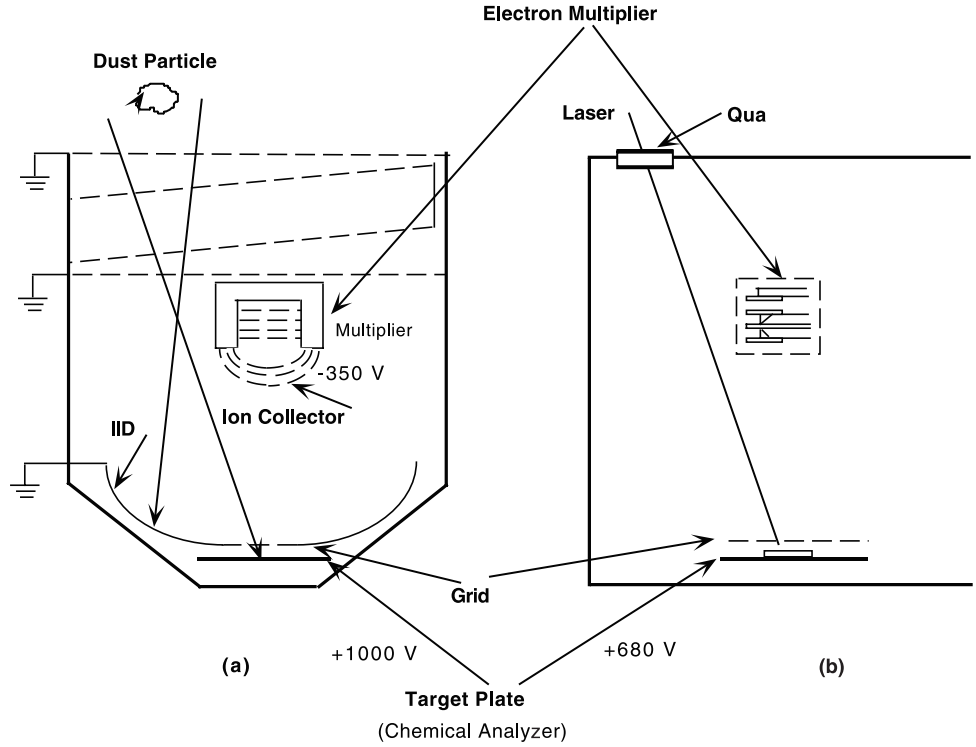

Figure 1. Schematics of (a) CDA instrument aboard Cassini mission which is simulated by (b) laser ionization time-of-flight mass spectrometer.

stacked dynodes that upon electrostatic capture of positive ions yield a high electron current gain and time resolutions of 10^{-8}s. The output of the CSA is in the form of an integrated charge pulse. The pulse has steps that correspond to the arrival time of different ionic species, whereas arrival time appears in the form of separate (differentiated) peaks for the electron multiplier.

[4] For interpretation of the TOF mass spectra returned from CDA aboard the spacecraft, there is a need to determine the instrument calibration, to understand the impact ionization process, and to characterize the impact-induced mass spectra over a range of particle sizes and impact velocities for a range of mono- and polymineralic targets, each having cosmochemical relevance. Previously, calibration with dust particles (of known compositions) have employed particles 0.2 to 20 μm diameter (mass of 10^{-15} to 10^{-10} g) that were electrostatically accelerated [*Grün et al.*, 1992] to velocities in the range of 1 to 70 km/s. Particles that can be accelerated by this method must be electrically conducting, or coated with a conducting (metal or carbon) film [*Stubig et al.*, 2001]. This experimental methodology also requires that the projectiles be highly charged. Recently we have reported that the particle charge may result in consequences for the production of impact ionization (D. E. Austin et al., Hypervelocity microparticle impact studies using a novel cosmic dust mass spectrometer, submitted to *Journal of Geophysical Research*, 2002).

[5] To simulate the pulsed ion-source of a dust particle impact upon the Rh target plate of the CDA instrument, our initial calibration program was initiated using a pulsed laser focused on to a mono- or poly-mineralic sample. Figure 1 shows the correspondence between our laboratory laser ionization time-of-flight mass spectrometer (the mock-up instrument) and the CDA instrument aboard the Cassini spacecraft. Since the particle-target interaction times (∼10 ns) and the energies of dust particles are comparable to the duration and energies of available pulsed lasers [*Kissel and Krueger*, 1987], laboratory laser ionization experiments are useful to optimize the instrumentation for impact experiments. Because most of the energy of the laser pulse is absorbed by the material ablated in the first femtoseconds of laser-target interaction, the degree to which an incidence of laser pulse with a energy of 300 μJ focused on to the sample simulate an impact of particle is only approximately constrained. If one assumes that the laser pulse may produce effects comparable to impact then our incident laser energy density, 10^{11} W/cm^2, simulates the impact of particles of different densities and velocities, for example a particle (or projectile) having density of ∼8 g/cm^3 (Fe-Ni) moving at 23 km/s or a particle with density 1 g/cm^3 moving at 65 km/s. Figure 2 displays the range of particle impact velocities as a function of various particle densities (1.0 to 10 g/cm^3) that will simulate the energy density of our laser. For these calculations the particle/projectile footprint is taken to be 6.5 μm i.e. the focal diameter of the laser beam. Normally, particles having initial densities in ∼0.01 to 5 g/cm^3 range are expected to be encountered in space. That could range in composition from those similar to carbonaceous chondrites that are of low density and possibly correspond to the Brownlee particles [*Brownlee*, 1985] collected in the Earth's atmosphere to differentiated silicate and metal asteroid fragments.

[6] In the present paper, we describe our work on calibration of time-of-flight mass spectrometer, a mock-up of the chemical analyzer of CDA instrument. The calibration has been carried out using laser-ionization method.

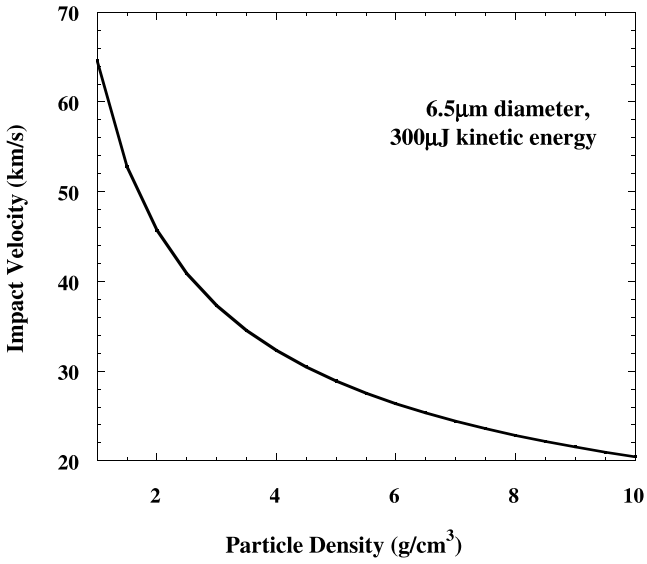

Figure 2. Velocity of 300 μJ kinetic energy, 6.5 μm diameter impacting particle as a function of particle density. Incident laser thus simulates an impact of Fe-Ni projectile (density ~8 g/cm^3) at 23 km/s. Velocity, V, here is calculated using $E = 0.5\ m_p V^2$ where m_p is particle mass, and E = 300 μJ.

Also, we have examined laser-ionization mass spectra of several minerals, viz., kamacite [Fe-Ni], pyrrhotite [FeS], olivine [Mg_2SiO_4], serpentine [$Mg_3Si_2O_7 \cdot 2H_2O$], and Murchison (meteorite).

2. Experiments

[7] The schematic diagram of the experimental setup is shown in Figure 3. The beam of a nitrogen laser (Laser Science, VSL337ND-S model 337201) with 337 nm wavelength, 300 μJ energy, and 4 ns pulse duration, is directed by two beam steerers (Newport, model BSD-1) into the vacuum chamber through a quartz window (MDC, quartz Viewport no. 450020). The laser is focused with a 2.54 cm diameter plano-convex fused silica lens (Newport, SPX022AR10) to a spot diameter of ~6.5 μm onto the sample mounted on the target plate of the mock-up instrument. The focal length of the lens is 10 cm. To minimize the loss of laser intensity, the lens has anti-reflection coating in the UV region and the mirrors of the beam steerers have dielectric coatings to give 99% reflectivity in the UV region.

[8] The mock-up instrument consists of a target plate of commercial aluminum alloy, a copper grid having 66% transmission, an aluminum grid having 78% transmission and a positive ion detector. All these are mounted parallel to each other on a 35 cm long rail and their distances relative to each other can be varied. The spacing between the target plate and the copper grid is variable between 0.3 and 0.6 cm between the copper grid and the aluminum grid is ~20 to 30 cm, and between the aluminum grid and detector is ~1 cm. Samples of a few mm diameter and 0.10 to 0.15 mm thickness are mounted on the target plate in a circle about 2 cm from the center. The target plate can be remotely rotated about its center by the required angle in steps of one degree using a stepper motor (Figure 4). Thus, any sample or a new surface of the sample can be brought remotely to the focal spot of the laser beam. This arrangement allows recording of spectra of many samples in one set of experiments without breaking vacuum. The chamber pressure was maintained below 1.0×10^{-6} mbar with a 1500 l/s diffusion pump.

[9] When a laser pulse is focused on to the solid target, it creates a localized high-temperature region resulting in vaporization and partial ionization of the target material. For the present experiments, assuming that ~1% of the laser pulse energy, 3 μJ, is coupled to the hemispherical portion of the target (for example Fe) with diameter equal to the footprint of the laser (~7 μm), we estimate that the

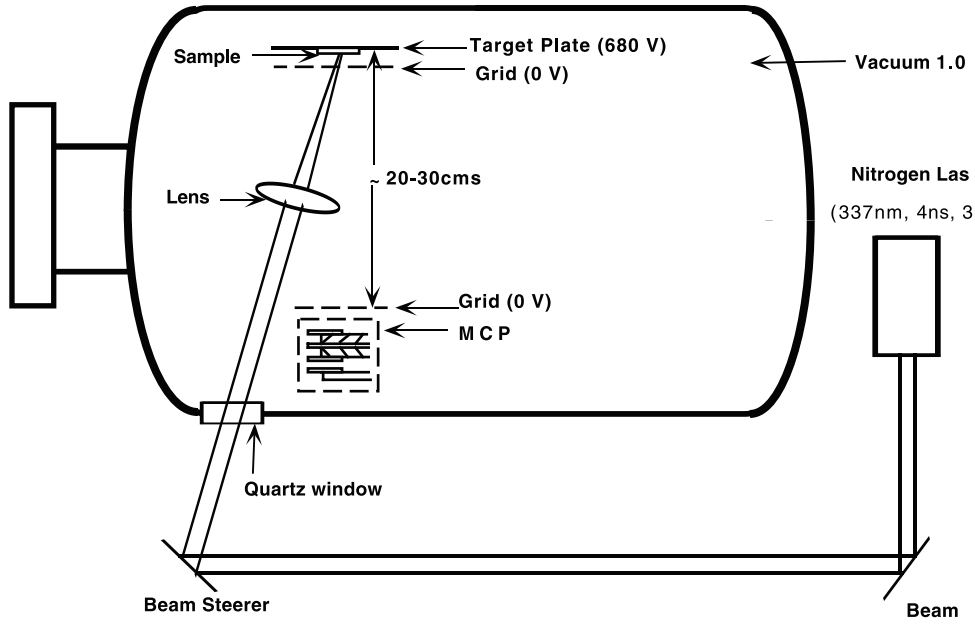

Figure 3. Schematic of optical setup for instrument. Laser beam is directed using beam steerers into vacuum chamber through a quartz window and then focused onto sample.

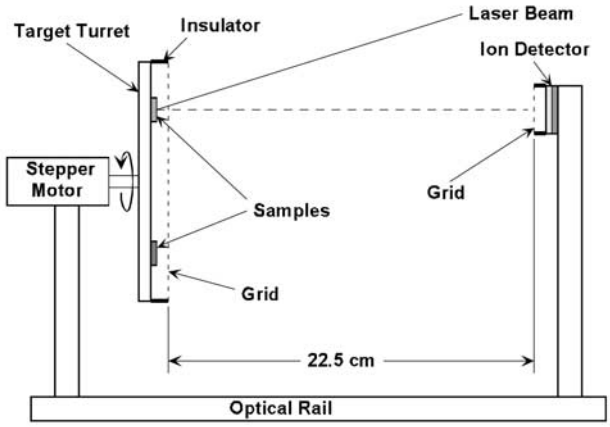

Figure 4. Schematic of mechanical assembly of experimental apparatus.

equivalent temperature rise in the irradiated material would be $\sim 10^4$ K. This estimate assumes that all the absorbed energy gets converted into the thermal energy of the material. This temperature, of course, is an upper estimate, as part of the laser pulse energy will go into vaporizing and ionizing the target material in the irradiated region. The resulting pulsed plasma expands as a plume normal to the target surface and enters the electric field between the target and the grid, where the positive ions and electrons (and negative ions) are separated by the electric field. The electrons (and negative ions) are collected by the target plate and detected by a charge sensitive amplifier. The magnitude of this (negative) electron charge gives the estimate of the total ionization taking place. If the sample material is an insulator, it is first coated with a thin conducting layer on all the sides and then fixed onto the target material using conducting paint so that electrons released due to ionization of the material are conducted away by the target plate and also do not disturb the electric field between the target plate and the grid. The positive ions are accelerated toward the grid. The velocities gained by different positive ions are inversely related to square root of their masses. After passing through the grid, these ions drift about 20 to 30 cm in the field-free region and reach the detector at different times.

[10] The time of arrival of a positive ion at the detector is given by the relation [*Cotter*, 1997]

$$t = L\sqrt{\frac{m}{2zV}},$$

where m is the ionic mass, z is the degree of ionization, L is the field free drift distance and V is the acceleration voltage between the target plate and the grid. The time of arrival of an ion at the detector is thus related to the ratio of its mass and its degree of ionization, m/z.

[11] Similar to that in CDA, we have employed two kinds of ion detection systems, i.e., a charge sensitive amplifier (CSA) with copper collector plate, and a multichannel plate (MCP) detector (Figure 5). However, these two detectors have not been used simultaneously but in separate experiments. With CSA detector, the collector plate was kept at ground potential, shielded in an aluminum enclosure to isolate it from electromagnetic noise. The collection area was limited to the ~6.8-cm-diameter central zone of the 15-cm-diameter copper collector plate. The charge collected by the copper plate is monitored by the charge sensitive amplifier (EG &G, ORTEC model 142A) which has a risetime of ~12 ns. The multichannel plate detector (Galileo Corp., part no. 1397-0050) has gain of $\sim 10^6$ and risetime of a few ns, which is comparable with that of MM1 multiplier used in CDA. The active detection diameter of the MCP is 18 mm and its operating voltage is kept at +1800 V. A preamplifier (EG&G, ORTEC model VT120C) is used for further amplifying the signal and for impedance matching with the 50 Ω input of the oscilloscope. Signals from both the detectors are recorded on a 500 MHz, HP54540 digital storage oscilloscope, which is triggered synchronously with the laser.

[12] The experiments have been conducted in two different configurations of the mass spectrometer. In the first (configuration-1), a voltage of 680 V is applied onto the target plate (grid grounded and hence it will accelerate positive ions toward it), the distance between the target plate and the grid is 6 mm, whereas the separation between the target and the detector is 280 mm. In the second (configuration-2), the corresponding voltage and distance values are 1000 V, 3 and 230 mm, respectively. In the second configuration, the mass spectrometer is similar to the Chemical Analyzer part of the CDA instrument aboard the Cassini mission [*Srama and Grün*, 1997]. The details of distances and voltages in each experiment are listed in Table 1. We wish to emphasize that the experiments done here are different from those often performed in conventional mass spectrometry for chemical analysis. In each of the present experiments, the mass spectrum resulting from a single laser pulse is recorded. Spectra from a number of laser pulses are not averaged as is customarily done in conventional TOF mass spectrometry. This has been done as the CDA instrument aboard Cassini is expected to send the mass spectra of individual particle impacts.

3. Results and Discussion

[13] We have carried out two sets of experiments. One set has been done in configuration-1 in order to examine the efficiency and the resolution of the instrument. The second set has been done to examine the mass spectra of some minerals of cosmochemical importance.

[14] In the first set of experiments, the mass spectra have been recorded in configuration-1 from aluminum alloy and stainless steel samples employing the CSA, and the aluminum alloy and the kamacite samples using the MCP detector. For the aluminum alloy, the target plate itself was treated as sample. Using the CSA, at low laser power densities, the temporal variation of charge indicates two steps corresponding to $^{23}Na^{+1}$ and $^{39}K^{+1}$ with approximately 350 ns risetime each. Presence of contaminant alkali salts on the sample surface is well known in mass spectrometry. The known mass of the Na^+ and K^+ ions is advantageously used for calibrating the instrument. With higher laser power density, a high-amplitude, long duration (~800 ns) step was observed (Figure 6a). This step in fact could be associated with the overlap of two signals, corresponding to the arrival of $^{23}Na^{+1}$ and $^{27}Al^{+1}$. No further

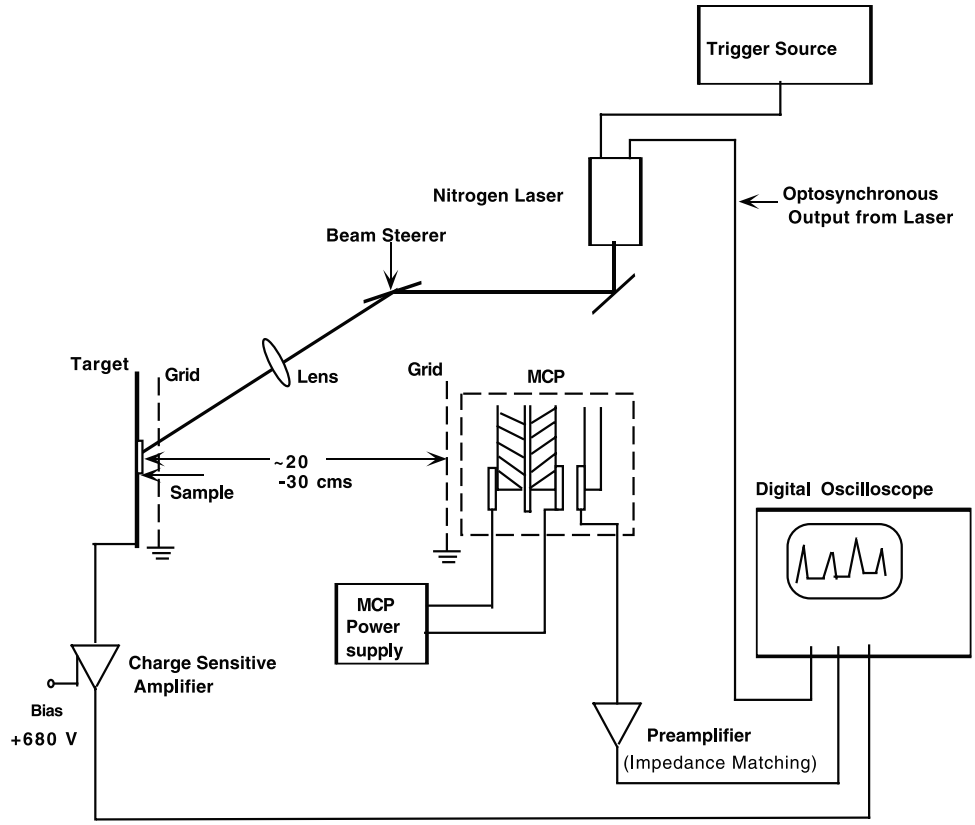

Figure 5. Experimental arrangement for data acquisition. With pulsed laser irradiation of the sample, +ve and −ve ions are generated. These are separated by the electric field between the plate and the grid. The −ve ions are collected by the plate and recorded by a charge sensitive amplifier. The +ve ions that are accelerated toward the grid drift about 20–30 cm in a field free region and are then collected by a detector (charge sensitive amplifier or multichannel plate). The detector signal is recorded using a fast digital oscilloscope.

steps were observed. This shows that ions separated by four daltons could not be resolved using the CSA detector. The TOF mass spectrum of the stainless steel sample is shown in Figure 6b. The spectrum displays only a single step of ~800 ns risetime. This step could be associated with an overlap of steps due to $^{56}Fe^{+}$, $^{52}Cr^{+}$ and $^{58}Ni^{+}$ ions. This demonstrates that the CSA detector in the chemical analyzer of CDA will not be able to resolve between the elements Fe and Ni. For this reason we have not used the CSA detector for further experiments on minerals. The electron charge collected at the target plate, which is a measure of the total ion yield is estimated to be around 4.7 and 2.8 pC for the aluminum alloy and stainless steel samples, respectively. The positive ion charge collected at the collector plate was estimated to be 0.23 and 0.15 pC for these two samples. This corresponds to an ion detection efficiency of 4–5% over a ~0.09 sr collection solid angle.

[15] Figure 7 displays the TOF mass spectra of the Al alloy and the kamacite recorded with the MCP detector. Figure 7a shows a well-defined Al^{+1} peak along with peaks corresponding to $^{23}Na^{+1}$ and $^{39}K^{+1}$ from surface impurities and peaks corresponding to Cu^{+1} and Mg^{+1} present at low

Table 1. Experimental Configurations

Experiment	Sample	Spacing, mm		Target Voltage, volts	Detector Type	Detector Voltage, volts
		Target to Grid	Grid to Detector			
1	Al alloy[a]	6.0 ± 0.5	280 ± 1	680 ± 10	CSA[b]	
2	Stainless steel	6.0 ± 0.5	280 ± 1	680 ± 10	CSA	
3	Kamacite	6.0 ± 0.5	280 ± 1	680 ± 10	MCP[c]	1800
4	Kamacite	3.0 ± 0.5	230 ± 1	1000 ± 10	MCP	1800
5	Pyrrohtite	3.0 ± 0.5	230 ± 1	1000 ± 10	MCP	1800
6	Olivine	3.0 ± 0.5	230 ± 1	1000 ± 10	MCP	1800
7	Serpentine	3.0 ± 0.5	230 ± 1	1000 ± 10	MCP	1800
8	Murchison Meteorite	3.0 ± 0.5	230 ± 1	1000 ± 10	MCP	1800

[a]Target plate made of Al alloy was itself treated as the sample.
[b]Charge collected on copper plate and measured using charge sensitive amplifier.
[c]Multichannel plate.

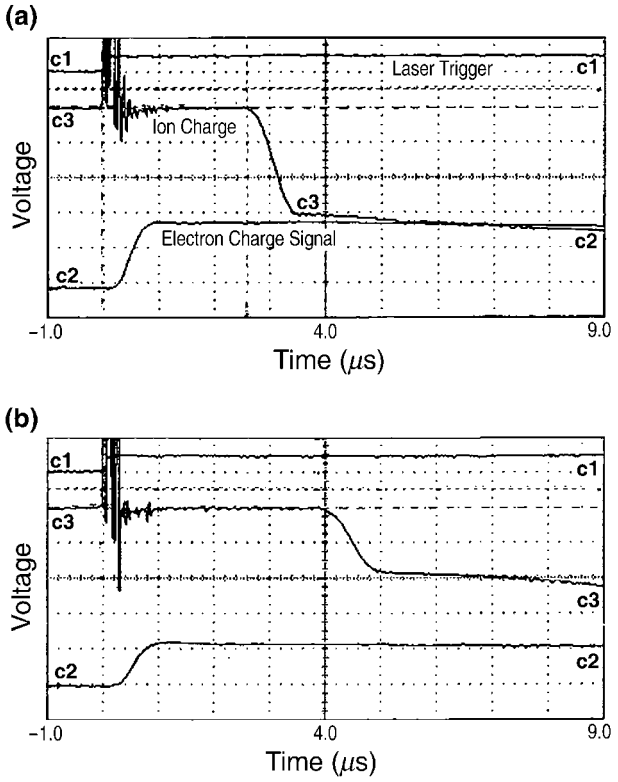

Figure 6. Single laser pulse time-of-flight spectra recorded in configuration-1 using charged sensitive amplifier: (a) from Al sample, (b) from stainless steel sample. Channel c1 displays the opto-synchronous output due to laser trigger (5 V/div). Channel c2 displays signal due to integrated electron charge collected at target plate (200 mV/div). Channel c3 displays ion signal at collector plate (75 mV/div).

levels of concentration as alloying elements. Figure 7b shows the spectrum for kamacite. Kamacite (94.5% Fe and 5.5% Ni) is the principal mineral in Fe-Ni meteorites. Meteorite Gibeon was the source of our sample. Here, too, we observe well-resolved peaks of $^{56}Fe^{+1}$ and $^{58}Ni^{+1}$. Yet another spectrum from this mineral recorded at slightly higher laser intensity (laser intensity was varied using neutral density filters) is shown in Figure 7c. Here, we see an additional peak corresponding to $^{60}Ni^{+1}$. These spectra show the presence of Na and Al, which are separated by 4 dalton, Na and Mg separated by 1 dalton, and Fe and Ni that are separated by 2 daltons as clearly resolved peaks. These data imply that the resolution of our instrument is 1–2 dalton in the range of 20 to 60 mass numbers.

[16] In the second set of experiments, TOF mass spectra have been recorded in configuration-2 on five materials comprising kamacite, pyrrhotite, olivine, serpentine, and Murchison meteorite. If the sample material is an insulator, it is first coated with a thin (~225Å) conducting (gold) layer on all the sides and then fixed onto the target material using conducting paint so that electrons released due to ionization of the material are conducted away by the target plate. Samples treated in this way included olivine, serpentine, and Murchison meteorite. The charge on the target plate is detected using the charge sensitive amplifier. The magnitude of this (negative) electron charge (channels c2, Figures 6a and 6b) gives the estimate of the total ionization taking place. Because of the shot to shot variation in the spectra, two representative spectra are given for each of the five minerals.

[17] Figure 8 shows the spectra for kamacite. Here, aside from the two peaks observed earlier from contaminants ($^{23}Na^{+1}$ and $^{39}K^{+1}$) a peak at 41 amu, which can be identified as $^{41}K^{+1}$, is also observed. The two isotopes of potassium, ^{39}K and ^{41}K having a natural abundance of 93.26 and 6.73%, respectively (Table 2), with the abundance ratio of 13.85, show a peak height ratio of 15 ± 2 and 16 ± 2, respectively in the two spectra. As expected from this mineral, both Fe and Ni peaks are seen. It is important to note here that though the ratio of Fe to Ni abundance in kamacite is ~17, the peak height ratios in the two spectra are 1.2 and 1.5 (Figures 8a and 8b). One of the factors contributing to this small peak height ratio in spite of this large Fe/Ni abundance ratio is the slightly higher ionization potential of Fe (7.87 eV) relative to that of Ni (7.64 eV) which leads to enhancement of Ni^{+1} ions and hence small Fe/Ni peak height ratio. Also, Ni has a natural concentration of 68.27% ^{58}Ni and 26.10% ^{60}Ni, so that the ratio of their

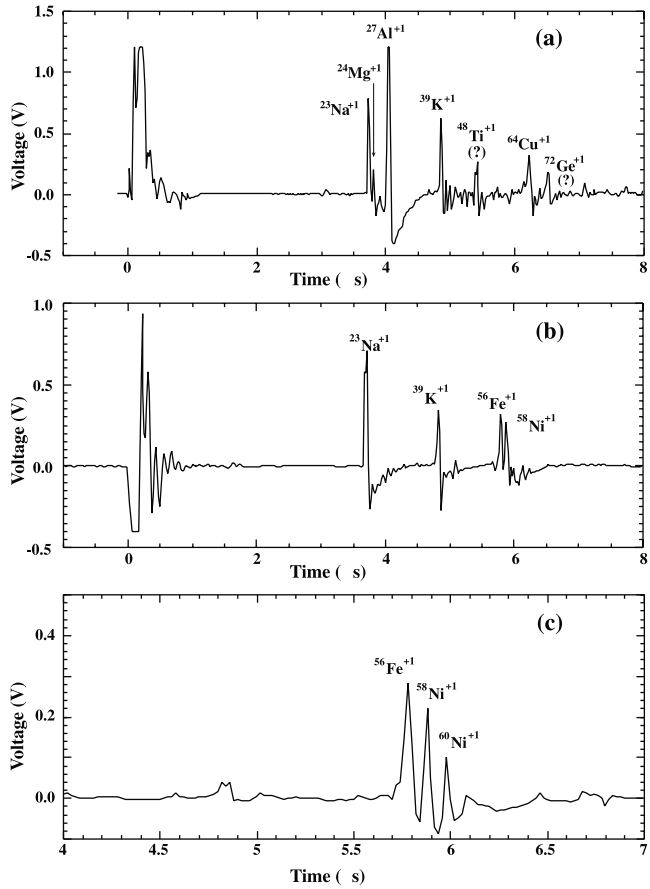

Figure 7. Single N_2 laser pulse, time-of-flight spectra recorded in configuration-1 using multichannel plate detector: (a) from commercial Al sample, (b) from kamacite, at laser power density of 3.45×10^9 W/cm^2, (c) from kamacite, at laser power density of 4.5×10^9 W/cm^2.

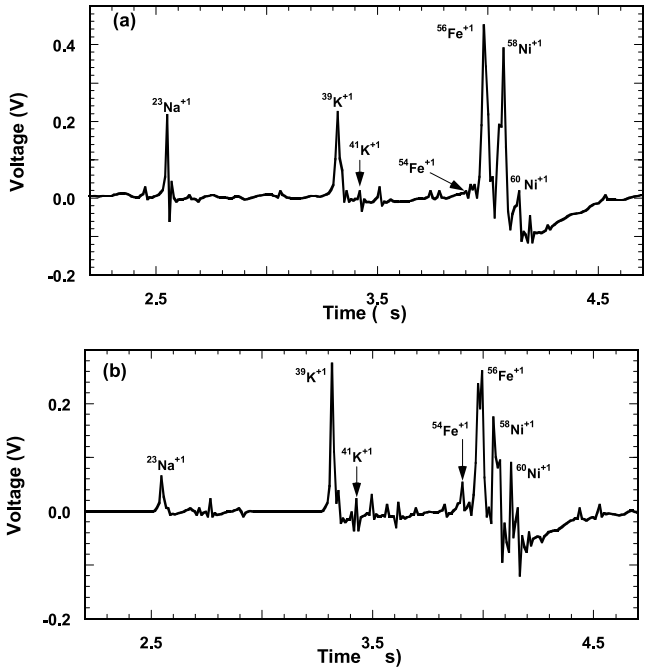

Figure 8. Typical single laser pulse time-of-flight spectra recorded in configuration-2 from kamacite (Fe-Ni).

cosmic abundances is 2.59. However, the ratios of the spectral peak heights due to ions of these isotopes from the two observed spectra are as high as 35 and as low as 2.0. Similarly, for iron, the natural abundance of the two isotopes ^{56}Fe and ^{54}Fe being 91.8 and 5.8%, the abundance ratio is 15.8 but the ratio of the peak heights for these isotopes from the two observed spectra are 24 and 5.3, respectively. Both the spectra show a peak at 55 amu, which could be due to the presence of $^{55}Mn^{+1}$ ions.

[18] The mass spectra of pyrrohtite (FeS) are shown in Figure 9. This mineral gives prominent iron peaks in its spectrum. Figure 9a shows $^{54}Fe^{+1}$ and $^{56}Fe^{+1}$ peaks. The peaks due to sulfur ions are not seen. This is expected, as sulfur forms negative ions due to its large ionization potential and its affinity toward an electron (Table 2). Negatively charged sulfur ions will get collected at the target plate along with the electrons. An unidentified peak at mass number 29 might be Fe^{+2}. In Figure 9a the ^{56}Fe to ^{54}Fe peak height ratio is $\sim 6 \pm 1$. In the second spectrum (Figure 9b), we observe that $^{56}Fe^{+1}$ and $^{57}Fe^{+1}$ peak heights are comparable even though ^{57}Fe has a natural abundance of 2.1% as compared to ^{56}Fe with a natural abundance of 91.8%.

[19] Olivine, (Mg, Fe)SiO_4, yields spectra as shown in Figure 10. Figure 10a shows a very well defined peak from

Table 2. Physical Properties of Elements and Their Chemical Abundances

Element	Mass Number, Amu	Isotopic	Abundance, %	Melting Point, °C	Boiling Point, °C	Ionization Potential, eV	Electron Affinity, eV
H	1.00797	^{1}H	99.985	−259.14	−252.87	13.598	0.747
		^{2}H	0.015				
		^{3}H	0.0				
C	12	^{12}C	98.89	3550	4827	11.26	
		^{13}C	1.11				
O	15.9949	^{16}O	99.76	−218	−182.96	13.618	1.466
		^{17}O	0.04				
		^{18}O	0.20				
Na	22.98	^{23}Na	100	97.81	882.9	5.139	
Mg	24.305	^{24}Mg	78.99	648.8	1090	7.646	
		^{25}Mg	10.00				
		^{26}Mg	11.01				
Al	26.9815	^{27}Al	100	660.37	2467	5.986	
Si	28.0855	^{28}Si	92.23	1410	2355	8.151	
		^{29}Si	4.67				
		^{30}Si	3.10				
S	32.064	^{32}S	95.0	112.8	444.6	10.361	2.07
		^{33}S	0.76				
		^{34}S	4.22				
		^{38}S	0.02				
K	39.0983	^{39}K	93.26	63.25	759.9	4.341	
		^{40}K	0.01				
		^{41}K	6.73				
Ca	40.08	^{40}Ca	96.941	839	1484	6.113	
		^{42}Ca	0.647				
		^{43}Ca	0.135				
		^{44}Ca	2.068				
		^{46}Ca	0.004				
		^{48}Ca	0.187				
Fe	55.847	^{54}Fe	5.8	1535	2750	7.870	
		^{56}Fe	91.8				
		^{57}Fe	2.1				
		^{58}Fe	0.3				
Ni	58.71	^{58}Ni	68.27	1453	2732	7.635	
		^{60}Ni	26.10				
		^{61}Ni	1.13				
		^{62}Ni	3.59				
		^{64}Ni	0.91				
Rh	102.9048	^{103}Rh	100	1966	3727	7.46	

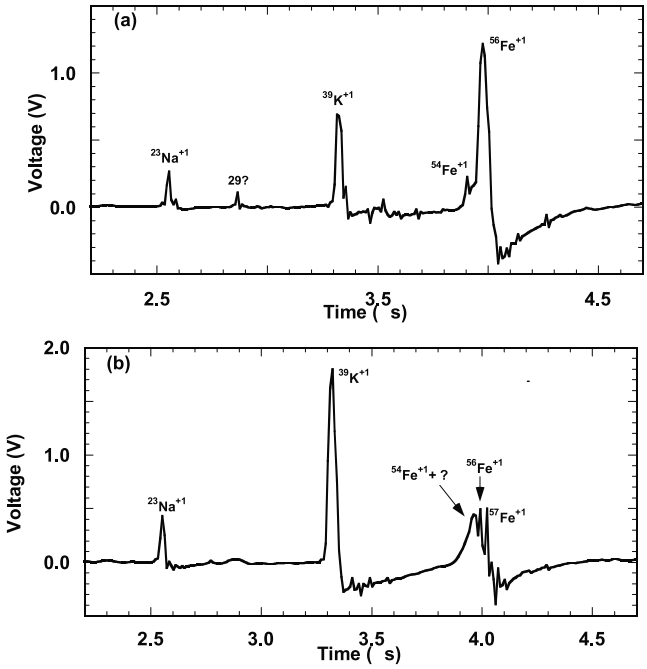

Figure 9. Typical single laser pulse time-of-flight spectra recorded in configuration-2 from pyrrhotite (FeS).

^{24}Mg as well as ^{26}Mg. Isotopes ^{24}Mg and ^{26}Mg, which have abundance percentage of 78.99 and 11.01% respectively (giving a ratio of 7.17), show a $^{24}Mg^{+1}/^{26}Mg^{+1}$ peak height ratio of 5 ± 1. A $^{41}K^{+1}$ peak also is observed. Peaks at 56 and 57 daltons can be assigned to $^{56}Fe^{+1}$ and $^{57}Fe^{+1}$. This peak height ratio $^{56}Fe^{+1}/^{57}Fe^{+1}$ is 4 ± 1. The spectrum shown in Figure 10b is similar to that in Figure 10a except

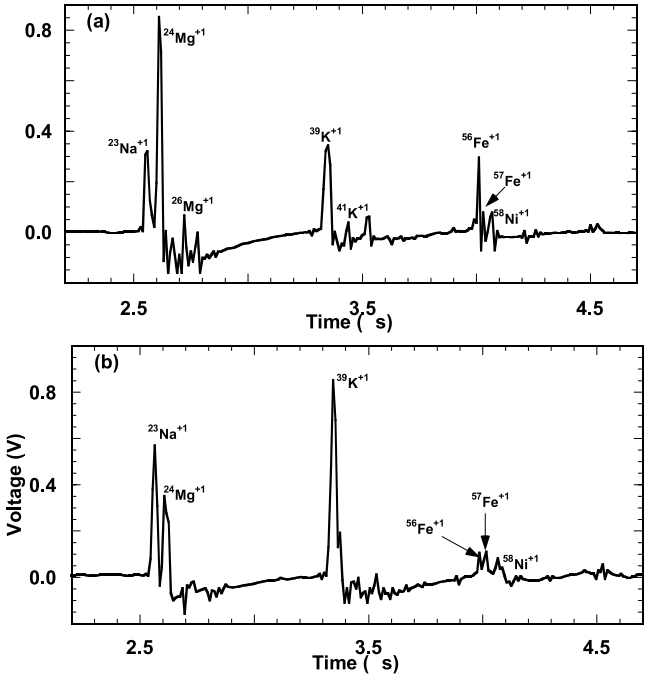

Figure 10. Typical single laser pulse time-of-flight spectra recorded in configuration-2 from olivine (Mg_2SiO_4).

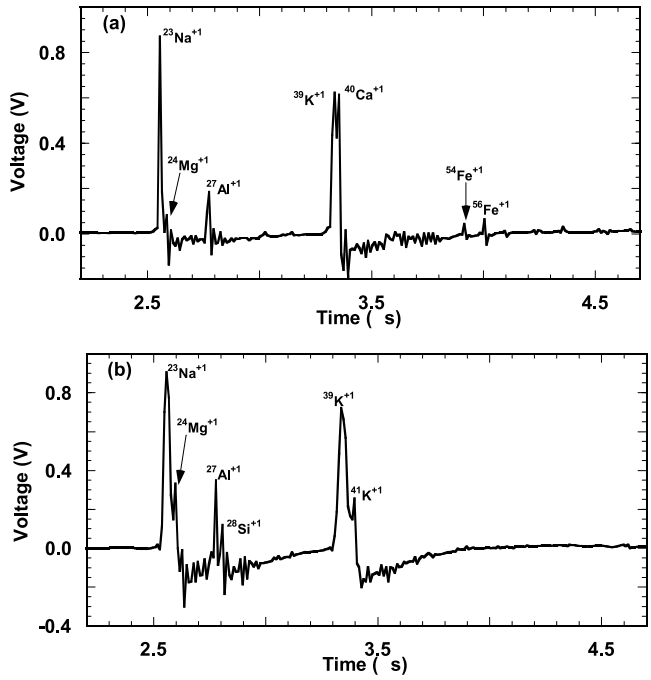

Figure 11. Typical single laser pulse time-of-flight spectra recorded in configuration-2 from serpentine ($Mg_3Si_2O_7 \cdot 2H_2O$).

that ^{26}Mg and ^{41}K isotope peaks are not observed. Peak heights corresponding to $^{56}Fe^{+1}$ and $^{57}Fe^{+1}$ at 57 amu (not identified) are comparable in this spectrum. The peak height ratio $^{24}Mg^{+1}/^{56}Fe^{+1}$ in the two spectra are 3.06 and 3.45, respectively. A small peak at 58 amu in both the spectra implies the presence of Ni impurity in the sample. Silicon and oxygen peaks are not observed. However, oxygen, like sulfur, is expected to form negative ions and will not be accelerated toward the MCP detector.

[20] Two spectra from the serpentine sample ($Mg_3Si_2O_7 \cdot 2H_2O$) are shown in Figure 11. In Figure 11a, the spectrum shows $^{24}Mg^{+1}$ and also iron isotopes $^{54}Fe^{+1}$ and $^{56}Fe^{+1}$. In addition, peaks are observed at 27 and 40 amu, which correspond to $^{27}Al^{+1}$ and $^{40}Ca^{+1}$, respectively. This implies that the sample contains aluminum and calcium impurities. In the second spectrum, Figure 11b, apart from $^{23}Na^{+1}$, $^{39}K^{+1}$, $^{27}Al^{+1}$, $^{24}Mg^{+1}$ and $^{41}K^{+1}$ peaks, we observe a weak peak at 28 amu that could belong to $^{28}Si^{+1}$. A hydrogen peak is not observed in either spectrum.

[21] Finally, spectra from the Murchison meteorite sample are shown in Figure 12. Figure 12a shows peaks corresponding to $^{24}Mg^{+1}$, $^{40}Ca^{+1}$ (present as a shoulder on the right side of the $^{39}K^{+1}$ peak), $^{56}Fe^{+1}$ and $^{58}Ni^{+1}$. The other spectrum (Figure 12b) shows a strong peak for $^{24}Mg^{+1}$, a weak peak for $^{58}Ni^{+1}$, and $^{40}Ca^{+1}$ peak, which is overlapping with $^{41}K^{+1}$ peak on its left shoulder. It is observed that some peaks grow at the expense of other peaks; for example, presence of a very strong peak of ^{24}Mg in Figure 12b is marked by the absence of ^{56}Fe peak as compared to that in Figure 12a.

[22] We observe that in a spectrum obtained from irradiation of a single laser pulse on a sample, the peak height for an element is not proportional to the abundance of that element in the material. This could be due to different

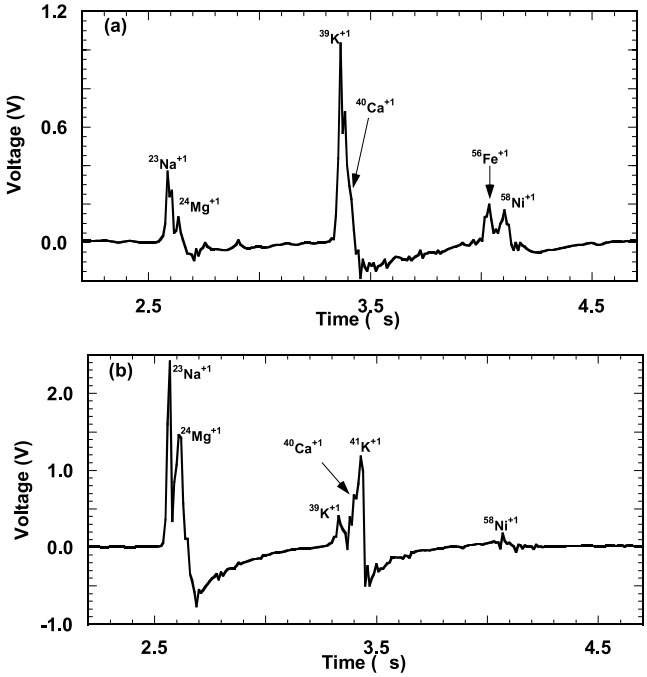

Figure 12. Typical single laser pulse time-of-flight spectra recorded in configuration-2 from Murchison meteorite sample.

ionization efficiencies of various elements, which depend not only on their ionization potentials but also on their bonding characteristics in a particular solid. However, the ratios of the spectral peaks corresponding to isotope of an element are also different than the ratio of their isotopic abundances. Generally the peak intensities of the minor isotopes are higher than that would be expected from the natural abundance of the isotopes. *Odom and Schueler* [1990] found that the intensity ratios of the spectral peaks of ^{113}In and ^{115}In isotopes (^{113}In/^{115}In) were not equal to the abundance ratio of ^{113}In and ^{115}In. Also these varied with increasing the gain of the detector, keeping the laser intensity constant. This was attributed to the non-linearity of the detector. In the present experiments, the detector gain and the laser intensity were kept constant. Also, the dynamic range of the MCP detector used in the experiments is high (>100) and its response is linear. The enrichment of the minor isotope of elements in laser-ablated plumes has been observed for boron [*Gupta et al.*, 1980; *Pronko et al.*, 1999] and gallium [*Pronko et al.*, 1999] previously. The mechanism of this enrichment process is not yet understood and is controversial [*Gupta and Naik*, 2001; *Pronko et al.*, 2001]. However, it has been proposed that the enrichment of the minor isotopes in the spectra results from the complicated interaction of the charged ion species in the laser plasma with intense magnetic field formed by laser just ahead of the plume expansion process [*Gupta et al.*, 1980].

4. Implication for CDA Instrument Aboard Cassini

[23] Results show that in a spectrum obtained from irradiation of a single laser pulse on a sample, the peak height for an element is difficult to relate to the abundance of that element in the material. This is due in large part to different ionization efficiencies of various elements, which depend not only on their ionization potentials but also on their bonding characteristics in a particular solid. Peak height ratios of different elements are different from shot to shot, which could result from the inhomogeneity at μm-length-scale in the specimen; and all the elements do not show up in a spectrum. For example, nickel and iron are easy to ionize, as these have lower ionization potentials, and are always present in the spectrum. Sulfur and oxygen are absent in our experiments. This is expected as both sulfur and oxygen have high ionization potential and greater electron affinity (Table 2). Atoms from these elements may form negative ions which are collected by the target plate along with the electrons. Only a small peak of Si is seen, whereas hydrogen, present in water of crystallization is not observed in any of the spectra. This implies that a single spectrum recorded by the CDA instrument aboard the Cassini mission would be able to identify many of the elements like Fe, Ni, Ca, Al, Mg, Na, K and their isotopes, but may not be able to detect S and silicate group elements Si and O, present in the Saturnian system's dust. The determination of the chemical composition of the impacting dust particles will benefit from the development of a detailed physical model which simulates the physical phenomena occurring during the impact, and includes estimates of ionization efficiencies.

[24] The present laboratory experiments show that the time duration for recording the complete time-of-flight mass spectrum is ~5–6 μs, which corresponds to the time of flight of the heaviest ion. In case the CDA instrument is impacted by two (or more) dust particles in quick succession within 5–6 μs, the recorded spectrum would be superposition of two (or more) spectra. Care will be needed to interpret such spectra.

5. Summary

[25] Using a 300 μJ, 4 ns, 337 nm laser, we have assembled a mock-up instrument of the Cassini CDA employing both the charge sensitive amplifier and multichannel plate detectors. In this instrument, with the charge sensitive amplifier as a detector, the elements with masses differing by 4 amu could not be distinguished. Similar experiments with the multichannel plate as detector provided well-resolved peaks for these ion signals. In addition, peaks could be observed from several elements that are present at low levels of concentration in the sample. With this mock-up instrument when the mass number of the element is in the range 20–60 amu, spectral peaks for mass numbers differing by 1 amu are usually resolved.

[26] The mock-up instrument has been employed to examine mass spectra for cosmochemically important materials, e.g., kamacite (Fe-Ni), pyrrhotite (FeS), olivine [$(Mg,Fe)SiO_4$], serpentine ($Mg_3Si_2O_7 \cdot 2H_2O$) and Murchison meteorite. It is observed that all the elements do not show up in a spectrum. For example, nickel and iron are easy to ionize and, if in the sample, are always present in the spectrum. In contrast to this, sulfur and oxygen are always absent. Si ionization efficiency is poor, whereas H, bound as water of crystallization, appears hard to ionize. We observe that peak height for an element in a single pulse spectrum is

not proportional to the abundance of that element in the material. This could be due to different ionization efficiencies of various elements, which depend not only on their ionization potentials but also on their bonding characteristics in a particular solid. This implies that a single spectrum recorded by the CDA instrument aboard the Cassini mission would be able to identify the elements Fe, Ni, Ca, Al, Mg, Na, K and their isotopes, but may not be able to detect S and silicate group elements Si and O, expected to be present in the Saturnian system's dust.

[27] The present calibration data will help to identify the elements and isotopes of the impacting dust particle from the data expected from the CDA instrument. However, for determination of the chemical composition of the dust particle, our present knowledge of impact ionization efficiencies of an element in various minerals and detailed understanding of the physics of impact vaporization and ionization in materials is incomplete.

[28] **Acknowledgments.** Research supported by NASA and DOE. We thank V. Nenow for developing the sample-rotating fixture. We appreciate the helpful comments of two reviewers. Thanks are due to R. Srama, E. Grün, J. Bradley, and S. K. Sikka for their interest and encouragement. Contribution 8872, Division of Geological and Planetary Sciences (Caltech).

References

Brownlee, D. E., Cosmic dust: Collection and research, *Annu. Rev. Earth Planet. Sci.*, *13*, 147–173, 1985.

Cotter, R. J., *Time-of-Flight Mass Spectrometry*, Am. Chem. Soc., Washington, D.C., 1997.

Grün, E., H. A. Zook, H. Fechtig, and R. H. Giese, Collisional balance of the meteoritic complex, *Icarus*, *62*, 244–272, 1985.

Grün, E., H. Fechtig, M. S. Hanner, J. Kissel, B.-A. Lindblad, D. Linkert, G. Linkert, G. E. Morfill, and H. A. Zook, The Galileo Dust Detector, *Space Sci. Rev.*, *60*, 317–340, 1992.

Gupta, P. D., and P. A. Naik, Comment on "Isotopic enrichment in laser ablated plumes and commensurately deposited thin films," *Phys. Rev. Lett.*, *86*, 1386, 2001.

Gupta, P. D., R. Bhatnagar, and D. D. Bhawalkar, Isotopic enhancement in laser-produced plasmas, *J. Appl. Phys.*, *51*, 3422–3423, 1980.

Kissel, J., and F. R. Krueger, Ion formation by impact of fast dust particles and comparison with related techniques, *Appl Phys. A*, *42*(1), 69–85, 1987.

Odom, R. W., and R. Schueler, Laser microprobe mass spectroscopy: Ion and neutral analysis, in *Laser and Mass Spectrometry*, edited by D. A. Lubman, Oxford Univ. Press, New York, 1990.

Pronko, P. P., P. A. Van Rompay, Z. Zhang, and J. A. Nees, Isotope enrichment in laser-ablation plumes and commensurately deposited thin films, *Phys. Rev. Lett.*, *83*, 2596–2599, 1999.

Pronko, P. P., P. A. Van Rompay, Z. Zhang, and J. A. Nees, Reply to comment on "Isotope enrichment in laser-ablation plume and commensurately deposited thin films," *Phys. Rev. Lett.*, *86*, 1387, 2001.

Spilker, L. J., *Passages to a Ringed World*, *NASA Spec. Publ. SP-533*, 1997.

Srama, R., and E. Grün, The dust sensor for CASSINI, *Adv. Space Res.*, *20*, 1467–1470, 1997.

Stubig, M., G. Schafer, T. M. Ho, R. Srama, and E. Grün, Laboratory simulation improvements for hypervelocity micrometeorite impacts with a new dust, *Planet. Space Sci.*, *49*, 853–858, 2001.

T. J. Ahrens, Lindhurst Laboratory of Experimental Geophysics, Seismological Laboratory, California Institute of Technology, Seismological Laboratory 252-21, 1200 East California Boulevard, Pasadena, CA 91125, USA. (tja@caltech.edu)

J. L. Beauchamp, Arthur Amos Noyes Laboratory of Chemical Physics, California Institute of Technology, Pasadena, CA 91125, USA.

S. C. Gupta and G. Jyoti, High Pressure Physics Division, Bhabha Atomic Research Center, Mumbai 400085, India.